

Physical properties of Cr_2S_3 at high pressure

Lun Xiong(熊伦), Mingquan Jiang(江明全), Jinxia Zhu(竹锦霞), Lin Xia(夏林), Hao Wang(王毫), Shenghan Zhang(张升瀚), Pengfei Tang(汤鹏飞), Zhiqiang Chen(陈志强), Sheng Jiang(蒋升), and Hongliang Dong(董洪亮)
Citation: Chin. Phys. B, 2026, 35 (**3**): 036103. DOI: 10.1088/1674-1056/ae1cb3
http://cpb.iphy.ac.cn; http://iopscience.iop.org/cpb

What follows is a list of articles you may be interested in

Pressure-induced amorphization and metallization in orthorhombic SiP

Qiru Zeng(曾琪茹), Youjun Zhang(张友君), Yukai Zhuang(庄毓凯), Linfei Yang(杨林飞), Qiming Wang(王齐明), and Yi Sun(孙熠)
Chin. Phys. B, 2025, 34 (**9**): 096102. DOI: 10.1088/1674-1056/add4f6

First-principles study on structural, electronic, and superconducting properties of Laves-phase alloy $HfZn_2$ under pressure

Xiao Ma(马晓), Tao Wang(王涛), Jianfeng Wen(文剑锋), Zhenwei Zhou(周振玮), and Hongyu Zhu(朱红玉)
Chin. Phys. B, 2025, 34 (**8**): 086108. DOI: 10.1088/1674-1056/ade5a1

Structural evolution and bandgap modification of a robust mixed-valence compound $Eu_9MgS_2B_{20}O_{41}$ under pressure

Boyang Fu(符博洋), Wenfeng Zhou(周文风), Fuyang Liu(刘扶阳), Luhong Wang(王鲁红), Haozhe Liu(刘浩哲), Sheng-Ping Guo(郭胜平), and Weizhao Cai(蔡伟照)
Chin. Phys. B, 2025, 34 (**8**): 086102. DOI: 10.1088/1674-1056/add4e1

Morphology-tuned phase transition of MnO_2 nanorods under high pressure

Xue-Ting Zhang(张雪婷), Chen-Yi Li(李晨一), Hui Tian(田辉), Xin-Yue Wang(王心悦), Zong-Lun Li(李宗伦), and Quan-Jun Li(李全军)
Chin. Phys. B, 2025, 34 (**6**): 066105. DOI: 10.1088/1674-1056/adc192

Alloying and magnetic disordering effects on phase stability of Co_2 *Y*Ga (*Y*=Cr, V, and Ni) alloys: A first-principles study

Chun-Mei Li(李春梅), Shun-Jie Yang(杨顺杰), and Jin-Ping Zhou(周金萍)
Chin. Phys. B, 2022, 31 (**5**): 056105. DOI: 10.1088/1674-1056/ac3986

SPECIAL TOPIC — Structures and properties of materials under high pressure

Physical properties of Cr_2S_3 at high pressure

Lun Xiong(熊伦)[1,†], Mingquan Jiang(江明全)[1], Jinxia Zhu(竹锦霞)[1], Lin Xia(夏林)[1], Hao Wang(王毫)[2], Shenghan Zhang(张升瀚)[3], Pengfei Tang(汤鹏飞)[3], Zhiqiang Chen(陈志强)[3], Sheng Jiang(蒋升)[4,‡], and Hongliang Dong(董洪亮)[3]

[1] *School of Intelligent Manufacturing, Sichuan Institute of Arts and Science, Dazhou* 635000, *China*
[2] *Center for High Pressure Science and Technology Advanced Research, Beijing* 100093, *China*
[3] *Center for High Pressure Science and Technology Advanced Research, Shanghai* 201203, *China*
[4] *Shanghai Synchrotron Radiation Facility, Shanghai Advanced Research Institute, Chinese Academy of Sciences, Shanghai* 201204, *China*

(Received 12 August 2025; revised manuscript received 24 October 2025; accepted manuscript online 7 November 2025)

The compressive behavior of Cr_2S_3 in a quasi-hydrostatic environment was investigated by synchrotron x-ray diffraction using silicone oil as the pressure-transmitting medium in a diamond anvil cell. The maximum pressure was 34 GPa. We found that Cr_2S_3 undergoes a structural phase transition at a pressure of 8.5 GPa and the bulk modulus before the phase transition was fitted to be 88 GPa, which corresponds to a bulk modulus of 67 GPa calculated by first-principles theory. In addition, we also investigated the electrical resistance of Cr_2S_3 at different pressures and temperatures and found that the resistance decreases rapidly with increasing pressure or temperature and then remains almost unchanged with an increase in pressure or temperature. This indicates that Cr_2S_3 undergoes a structural phase transition around 8 GPa. In order to accurately confirm the phase transition pressure, high-pressure Raman experiments were used. We found that the position of Raman peak 3 increases approximately linearly at low pressure and remains constant above 8 GPa, indicating that a structural phase transition occurs at 8 GPa. Finally, the deviatoric stress of Cr_2S_3 at high pressures was investigated by the linewidth analysis method. The results show that the deviatoric stress increases approximately linearly at low pressures in the range of 2.8–6.2 GPa.

Keywords: Cr_2S_3, high pressure, equation of state, resistance, Raman scattering

PACS: 61.05.cp, 07.35.+k, 64.30.Jk, 72.90.+y

DOI: 10.1088/1674-1056/ae1cb3 **CSTR:** 32038.14.CPB.ae1cb3

1. Introduction

As an important layered transition metal sulfide, Cr_2S_3 possesses a series of novel physical properties such as ferromagnetism, semiconductivity and thermoelectricity under specific conditions. It is well known that Cr_2S_3 has a ferromagnetic Néel temperature of about 130 K and a Curie temperature of about 180 K, as well as ferromagnetic properties.[1]

Cr_2S_3 has two crystal structures, tripartite and rhombohedral, under ambient conditions, with the corresponding space groups *P*-31*c* and *R*-3, respectively. In the case of the rhombohedral structure, for example, the sulfur atoms first form the structural skeleton by dense hexagonal packing and then the chromium atoms occupy the octahedral voids of the S_6 octahedra. There are two cases in the filling process: a "CrS" layer consisting of CrS_6 octahedra shared by the edges is fully occupied and a "$Cr_{1/3}S$" layer shared by a third of the neighboring layers keeps the structure stable.[2] The electrical and magnetic properties of Cr_2S_3 can be controlled by varying the temperature and pressure due to the presence of chromium atomic vacancies in the metal layers.[3]

Previous high-pressure experimental and theoretical studies on Cr_2S_3 are very scarce. Li *et al.*[2] reported the structural and electrical transport results of Cr_2S_3 at high pressure, and the authors found that a structural phase transition occurred at 7–17 GPa. In order to further investigate the phase transition pressure of Cr_2S_3, *in situ* synchrotron radiation x-ray diffraction (XRD) experiments, electrical transport experiments and Raman scattering experiments with Cr_2S_3 at high pressures were carried out in a diamond anvil cell (DAC). In addition, the bulk modulus of Cr_2S_3 at ambient pressure and the Young's modulus at high pressures were obtained using first-principles calculations.

The sample of Cr_2S_3 used for the high-pressure experiments was purchased from Shanghai Aladdin Biochemical Technology Co., Ltd., and the purity of the sample was 99.99%. One of the structures of Cr_2S_3 is a rhombohedral structure (space group *R*-3; see left inset of Fig. 1) at ambient pressure and room temperature. Through scanning electron microscopy (SEM) tests, we found that the average grain size of Cr_2S_3 is about 10 μm (see right inset of Fig. 1). From this, we concluded that the Cr_2S_3 sample is a bulk material. From the diffraction patterns of Cr_2S_3 obtained by

†Corresponding author. E-mail: 1094129778@qq.com
‡Corresponding author. E-mail: jiangs@sari.ac.cn

© 2026 Chinese Physical Society and IOP Publishing Ltd. All rights, including for text and data mining, AI training, and similar technologies, are reserved.

Cu-target XRD (wavelength 1.5406 Å) at room temperature and ambient pressure (shown in Fig. 1), we found that the structure of Cr_2S_3 conforms to the rhombohedral structure with the space group *R*-3; the resulting cell parameters are $a = b = 5.9414(0.0009)$ Å and $c = 16.6756(0.0036)$ Å, with cell volumes of 509.7958(0.1225) Å^3. A T301 gasket was pre-pressed by a DAC to a thickness of ∼ 30 μm, and then a hole of diameter 120 μm was drilled in the center of the indentation by a laser drilling device. A ruby chip with a diameter of about 10 μm was used as a pressure sensor.[4] Silicon oil was chosen as the pressure-transmitting medium in the high-pressure XRD experiments.

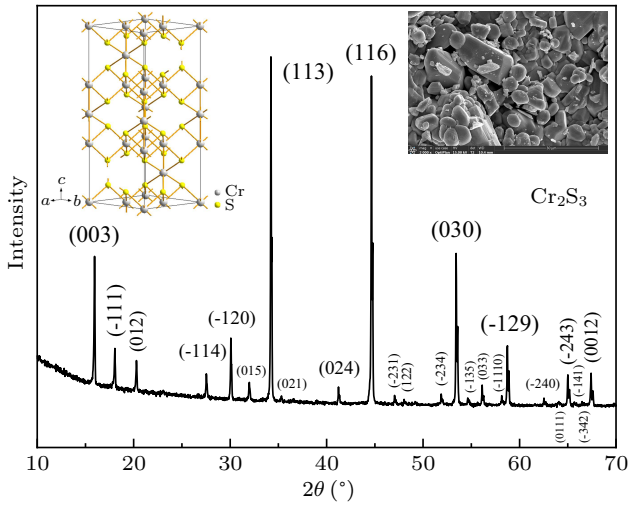


Fig. 1. The XRD (x-ray wavelength is $\lambda = 1.5406$ Å) spectrum of the powdered copper target of Cr_2S_3 at room pressure and it is well indexed to the rhombohedral structure for each diffraction peak; the Miller indices are indicated in the figure. The left inset is the crystal structure of the investigated Cr_2S_3 at ambient pressure and room temperature, and the right inset is a SEM image of the Cr_2S_3 sample.

In situ synchrotron XRD (wavelength 0.6199 Å) high-pressure experiments were performed at the BL15U1 beamline of the Shanghai Synchrotron Radiation Facility. Diffraction patterns at high pressures were received by a MarCCD detector, and the detector tilt angle and detector-to-sample distance were calibrated by a CeO_2 standard sample. The corresponding exposure time for all diffraction patterns was 10 s. The diffraction spectra acquired by the MarCCD at different pressures were then processed by Fit2d software,[5] resulting in integral spectra of diffraction angle and diffraction intensity.

Cr_2S_3 was subjected to *in situ* high-pressure and low-temperature electrical transport measurements in a DAC. To load the samples into the DAC, a T301 gasket was pre-indented to a thickness of approximately 30 μm. Then, a sample hole with a diameter of 250 μm was drilled in the middle of the gasket indentation. A thin layer of cubic boron nitride (cBN) was pressed onto the gasket to insulate the electrode from the gasket. A 130 μm diameter hole was then drilled in the middle of the cBN and the Cr_2S_3 powder sample was loaded into the DAC. To ensure good electrical conductivity between the electrode and the sample, and to prevent the possible introduction of impurities and electrode short-circuiting, no pressure-transmitting medium was added in the experiment. DC impedance was used to measure electrical transmission.[6] The method was to connect two electrodes to the sample and measure the DC impedance in the DAC. The DC impedance spectra were measured using a CS353 impedance analyzer (Wuhan Corette Instrument Co., Ltd.) and the measurement frequency range was from 0.01 Hz to 10 MHz. After modeling the data, the sample resistance can be measured in Ohms. Based on the above method, the resistance of Cr_2S_3 can be measured at different pressures and temperatures.

Raman spectra of backscattered structures were measured by an Acton SpectraPro 500i spectrometer with a liquid nitrogen-cooled charge-coupled device (CCD) detector (Princeton Instruments, 1340 × 100 pixels). The samples were excited by a diode-pumped frequency-doubled neodymium-doped vanadate laser ($\lambda = 532$ nm) with a focused beam diameter of 2–3 μm. Raman spectra were obtained by backscattering through a 1800 grooves/mm holographic grating with a resolution of about 2 cm^{-1}. Sample images were acquired by achromatic lenses and then focused onto a CCD detector for visual monitoring.

The Vienna *Ab-initio* Simulation Package (VASP) program[7] is used to perform density functional theory (DFT) calculations. The exchange–correlation is handled using the Perdew–Burke–Ernzerhof function in the generalized gradient approximation (GGA).[8] The projected additional plane wave (PAW) pseudopotential[9] with a kinetic energy cutoff of 500 eV is used to describe the expansion of the electronic eigenfunctions. The Monkhorst–Pack *k*-points are sampled from the Brillouin zone integration at the center of Γ and are 7 × 7 × 7. All atomic positions are fully relaxed until the energies and forces reach the tolerances of 1×10^{-5} eV and 0.02 eV/Å, respectively. Long-range interactions[10] are treated using the dispersion-modified DFT-D method.

Synchrotron XRD images were analyzed by Fit2d software.[5] The diffraction spectra integration plots at different pressures are shown in Fig. 2(a). The pressures were obtained using a ruby pressure marker.[4] The maximum pressure for the high-pressure experiments was 34 GPa. It can be seen that the diffraction peaks at low pressure can be well indexed to the rhombohedral structure with the space group *R*-3, and numerous diffraction peaks such as (-120), (113) and (116) are present. In addition, when the pressure was reduced from the highest pressure to 0.1 GPa, the original rhombohedral structure of the Cr_2S_3 sample returned. However, as shown in Fig. 2(a), only the (113) diffraction peak undergoes splitting at 4.7 GPa and 6.2 GPa. One possible reason is that

the grain size of Cr_2S_3 is not uniform (3–20 μm; see the right inset of Fig. 1). Under non-hydrostatic stress, some larger grains can cause pressure discontinuity leading to the splitting of the (113) diffraction peak. Larger grains near the edge of the sample pores may withstand lower pressure, resulting in the (113) diffraction peak appearing at a smaller diffraction angle. Another possible reason is that the Cr_2S_3 sample experiences strong shear stress in the uniaxial compression direction leading to changes in the crystal structure. However, further research is required to confirm this.[11]

The peak positions of the (-111), (-120), (113) and (116) diffraction peaks were used to fit the cell parameters and volume of Cr_2S_3 at low pressure. The volume at high pressures clearly shows a discontinuity, which leads us to believe that the Cr_2S_3 sample undergoes a structural phase transition at 8.5 GPa. The compression data from the high-pressure XRD experiments in this work, the data reported by Li *et al.*[2] and the theoretical results obtained in the present work are shown in Fig. 2(b), from which it can be seen that the rhombohedral structure of Cr_2S_3 still exists at 7.5 GPa whereas an obvious structural phase transition occurs at a high pressure of 8.5 GPa. The function used to fit the cell parameters and volume at high pressures is the third order Birch–Murnaghan equation and is expressed as[12]

$$P = 1.5K_0\left[\left(\frac{V_0}{V}\right)^{\frac{7}{3}} - \left(\frac{V_0}{V}\right)^{\frac{5}{3}}\right] \times\left\{1+\frac{3}{4}(K_0'-4)\left[\left(\frac{V_0}{V}\right)^{\frac{2}{3}}-1\right]\right\}. \quad (1)$$

Here K_0, V_0 and K_0' are the bulk modulus, cell volume and first-order derivatives of the bulk modulus, respectively, under ambient conditions.

The bulk modulus and first-order derivatives of the bulk modulus of Cr_2S_3 obtained by the third-order Birch–Murnaghan fit in this work are $K_0 = 88(14)$ GPa and $K_0' = 12.8(8.5)$, respectively. In addition, 67 GPa is the bulk modulus calculated by DFT theory. It can be seen that the error between the experimental and theoretical values of Cr_2S_3 bulk modulus in the present work is 24%. There are two primary reasons for the significant discrepancy between the bulk modulus values obtained from experiments and theoretical calculations. Firstly, DFT transforms the actual multi-electron problem into a single-electron problem to compute the effective potential of a single electron, the total energy of the electron gas is solely a function of the electron density, and the corresponding density is the ground state density of a single particle. In the GGA approximation, the exchange–correlation energy is related to both the density and the density gradient. Furthermore, compared with the GGA approximation, the electron temperature in real materials under environmental conditions is not absolute zero.[13] Secondly, the significant discrepancy between the theoretical and experimental bulk modulus is attributed to the non-hydrostatic properties of the pressure medium. The DAC is a uniaxial stress device. True hydrostatic conditions can only be achieved when the sample is placed within a fluid pressure medium. At room temperature, no known pressure medium can maintain a fully hydrostatic environment above ∼ 13 GPa due to solidification under high pressure. It has long been recognized that the presence of non-hydrostatic stress introduces bias into equation of state (EOS) determinations from DAC measurements. In all cases, volumes derived from non-hydrostatic pressure curves exceed those from quasi-hydrostatic curves by 10%–20%, particularly for polycrystalline samples.[14]

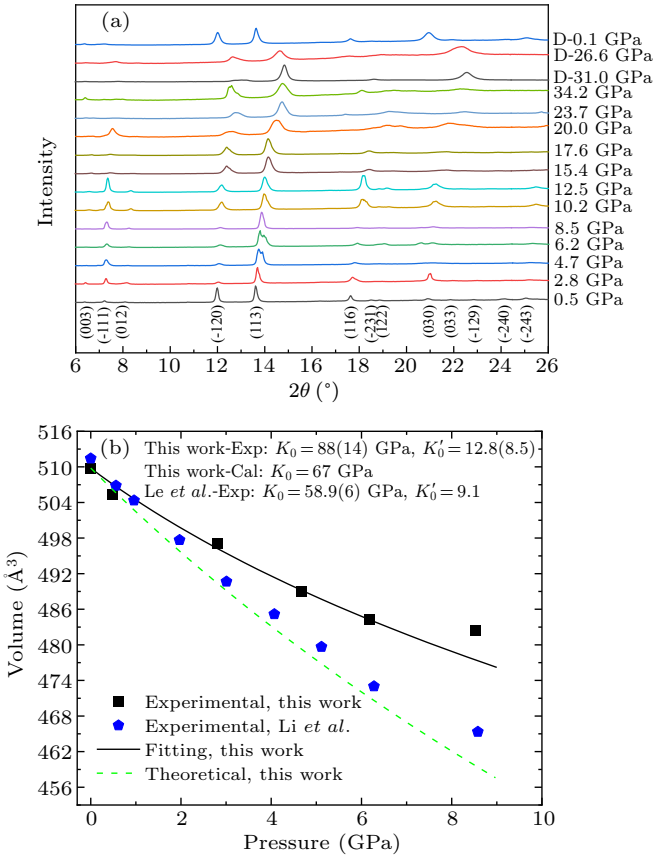


Fig. 2. (a) The effect of pressure on normalized XRD patterns of Cr_2S_3. D represents depressurization. (b) Compression curves of Cr_2S_3 at high pressure. The blue pentagons are the compression data obtained by Li *et al.*[2] The solid line is the fitted curve of the experimental data in this work and the dashed line is the fitted curve obtained from the theoretical calculations in this work.

A comparison of the ambient pressure bulk modulus and the first-order derivatives of the bulk modulus of Cr_2S_3 with those of the five halcogenides,[15–22] namely, Cr_2O_3, Bi_2O_3, Bi_2S_3, Sb_2O_3 and Sb_2S_3, is shown in Table 1. It can be seen that the bulk modulus of Cr_2S_3 is very close to that of Bi_2O_3,[17] much higher than those of Bi_2S_3,[18,19] Sb_2O_3[20] and Sb_2S_3,[21,22] but much smaller than that of Cr_2O_3.[15,16] The bulk modulus of Cr_2S_3 obtained in this work and Li *et al.*[2] is much higher than those of Bi_2S_3[18,19] and Sb_2S_3,[21,22] while that of Cr_2O_3[15,16] is much higher than

those of Bi_2O_3[17] and Sb_2O_3.[20] This is most likely because the bulk modulus of Cr (165 GPa)[23] is much higher than those of Bi (35.3–42.7 GPa)[24,25] and Sb (35.8 GPa).[26] Unfortunately, we have not solved the problem of the new structure after the phase transition at high pressure. In addition, we have tested the structure (γ-Cr_2S_3) reported by Li *et al.*[27] for indexing the high-pressure diffraction integrals of Cr_2S_3 and found that the structure is not consistent.

Table 1. A comparison of the results of different methods for calculating the bulk modulus (K_0) and the first-order derivative of the bulk modulus (K_0') for Cr_2S_3 and A_2X_3 (A = Cr, Bi, Sb and X = O, S).

Sample	Method	K_0 (GPa)	K_0'
Cr_2S_3	Present exp.	88(14)	12.8(8.5)
	Present calc.	67	–
	Exp.	59.8(6)[2]	9.1[2]
Cr_2O_3	Exp.	241(1),[15] 259(5)[16]	4.0(3),[15] 5.0(6)[16]
Bi_2O_3	Exp.	85.4(5)[17]	2.6(5)[17]
	Calc.	90.1(8)[17]	4.8(1)[17]
Bi_2S_3	Exp.	38.9(8),[18] 37.5(3)[19]	5.5(1),[18] 4.6[19]
	Calc.	36.5[18]	5.9[18]
Sb_2O_3	Exp.	20(1)[20]	9.4(1)[20]
Sb_2S_3	Exp.	37.6(1),[21] 26.91(14)[22]	–
	Calc.	32.2[21]	–

For the experiments in Fig. 3(a), we find that at low pressures (4.5 GPa and 7.8 GPa) the resistance decreases rapidly with increasing temperature and then remains almost constant. We believe that this is also a process of change from semiconductor to metal. After decompression from the highest pressure to 0.2 GPa, the sample becomes metallic, and as the temperature increases the resistance first decreases rapidly and then remains almost constant. Therefore, under low-pressure conditions (both compression and decompression), the resistance first decreases rapidly with increasing temperature and then remains unchanged. As can be seen in Fig. 3(b), the resistance decreases rapidly with increasing pressure at different temperatures and then remains constant. This phenomenon indicates that Cr_2S_3 undergoes a process of change from semiconductor to metal. In addition, at 8 GPa, the trend of decreasing resistance slows down rapidly. At this pressure, the Cr_2S_3 sample may have undergone a structural phase transition. After decompressing the Cr_2S_3 samples from the highest pressure to 13 GPa and 0.2 GPa one by one, the resistance values remained almost the same and showed metallic properties at all temperatures studied. In addition, we decompressed from the highest pressure to 0.2 GPa and then continued compression (see Fig. 4). It was found that the resistance remained metallic throughout, first decreasing rapidly and then remaining almost constant as the pressure increased. Pressure modifies the crystal structure or electronic structure, which results in a change in resistance. In addition, as the temperature increases, the amplitude and frequency of the thermal vibration of atoms in the metal lattice increase significantly with increasing temperature and the probability of collision of free electrons with the vibrating atoms during directional motion increases, leading to a shortening of the mean free path of the electrons and a decrease in the resistance.

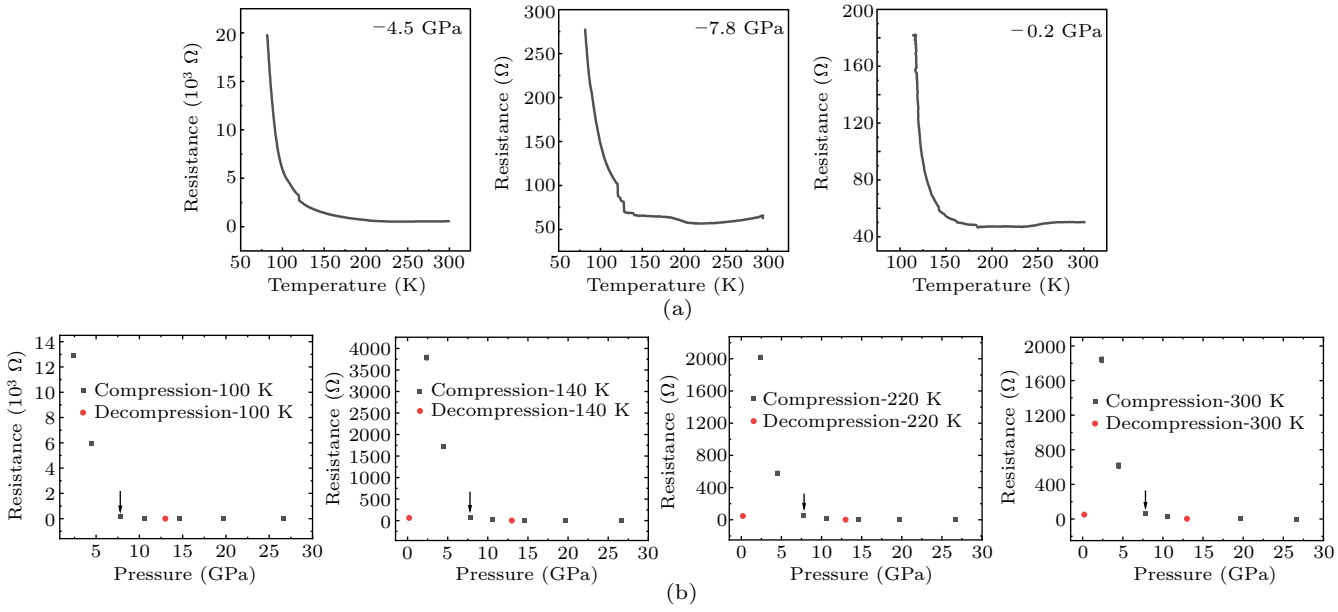


Fig. 3. (a) Variation of resistance with temperature of Cr_2S_3 at various pressures of 4.5 GPa, 7.8 GPa and 0.2 GPa. (b) Graph of the variation of resistance with pressure for Cr_2S_3 under various temperature conditions of 100 K, 140 K, 220 K and 300 K.

In order to investigate the phase transition pressure of Cr_2S_3, Raman experiments were conducted with pressures ranging from 0.6 GPa to 34.3 GPa. As shown in Fig. 5(a), some Raman peaks (1, 2, 3 and 4) in the range of 1350–3400 cm^{-1} can be clearly seen. In the low-pressure range from 1.6 GPa to 7.2 GPa, the frequencies of Raman peaks 1, 2 and 3 are redshifted with increasing pressure (see Fig. 5(b)), which may be due to the distortion of CrS_6 octahedra.[28] Be-

sides, the splitting of peak 2 at around 3 GPa may also be attributed to a minor structural phase transition, specifically a slight distortion of CrS_6 octahedra. In particular, Raman peak 3 decreases its position from 4 GPa to 22 GPa. The position of Raman peak 1 decreases at low pressure and increases at 8 GPa. On the other hand, the peak position of Raman peak 4 first increases with pressure, remains constant after 8 GPa, then continues to increase from 15 GPa and finally decreases at 30 GPa. Based on the previous phenomena, we conclude that the Cr_2S_3 sample probably underwent a structural phase transition at 8 GPa. This phase transition pressure is consistent with that derived from the current XRD data (8.5 GPa) and resistance data (8.0 GPa). In addition, new phase transitions may occur at 15 GPa and 30 GPa, respectively, which need to be confirmed by future studies.

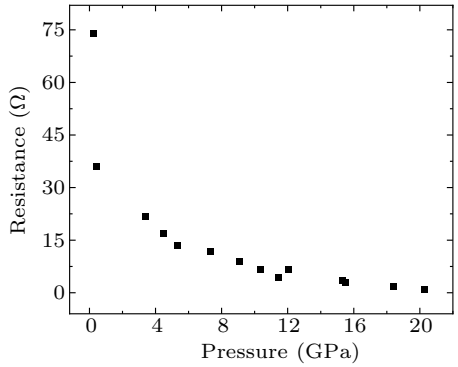


Fig. 4. The resistance trend chart of changes in resistance with increasing pressure after decompressing from the highest pressure and maintaining at room temperature for further compression.

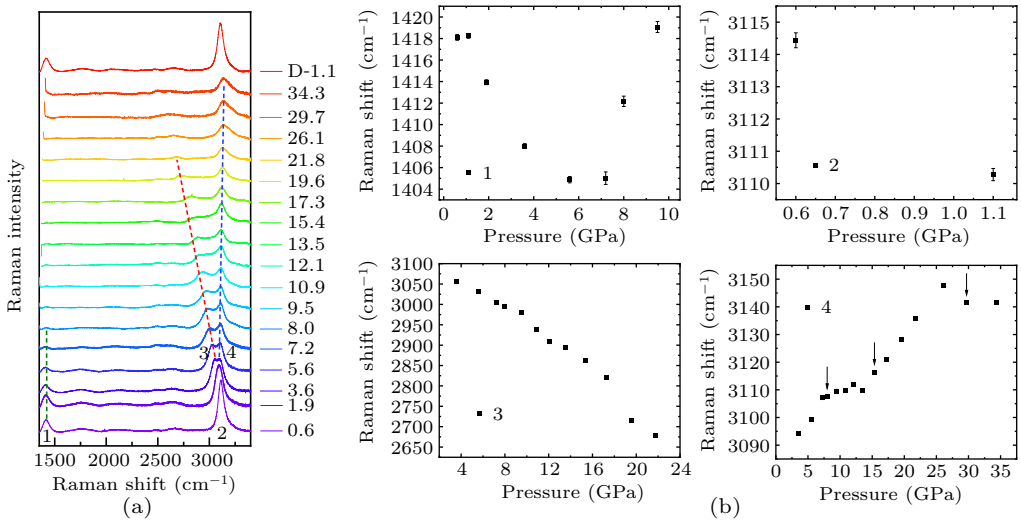


Fig. 5. (a) Representative Raman spectra of Cr_2S_3 under different pressures in the frequency range of 1350–3400 cm^{-1}. (b) Pressure-induced Raman shifts of peaks 1, 2, 3 and 4, respectively.

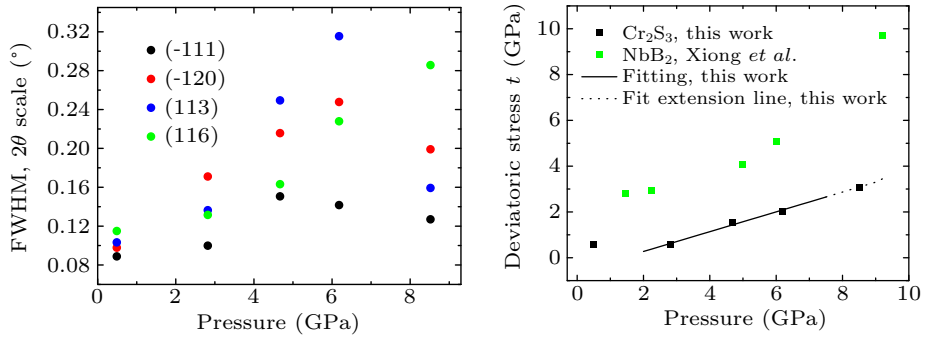


Fig. 6. (a) The FWHM of the diffraction peaks (-111), (-120), (113) and (116) of Cr_2S_3 at high pressures. (b) The variation of deviatoric stresses of Cr_2S_3 in this work and NbB_2 obtained from Ref. [27] with pressure.

The deviatoric stresses in materials at high pressures can be analyzed using the linewidth analysis theory proposed by Singh and his co-workers.[29] If 2ω is defined as the full width at half maximum (FWHM) of the diffraction peak on the 2θ scale, it follows that the microstrain η is

$$(2\omega_{hkl}\cos\theta_{hkl})^2 = (\lambda/D)^2 + \eta_{hkl}^2 \sin^2\theta_{hkl}, \tag{2}$$

where ω_{hkl}, D and λ are the FWHM of the diffraction peaks labeled with the corresponding *hkl* Miller indices (see Fig. 6(a)), grain size and synchrotron wavelength, respectively.

The deviatoric stress (strength) t can be expressed as

$$t \cong \langle\eta_{hkl}\rangle E/2. \tag{3}$$

The symbol $\cong$ in Eq. (3) means approximately equal or equal to, $\langle\eta_{hkl}\rangle$ means the average value of the diffraction peaks of η_{hkl} and E is the aggregated Young's modulus. Ac-

cording to Eq. (2), we can find that $(2\omega_{hkl}\cos\theta_{hkl})^2$ is linearly related to $\sin^2\theta_{hkl}$. Therefore, the microstrain η can be calculated from the slope of ηhkl^2 in Eq. (2). In addition, the deviatoric stresses at different pressures can be calculated from the Young's modulus at high pressures. The variation of the deviatoric stresses of Cr_2S_3 at high pressures is shown in Fig. 6(b). It can be seen that the strength of Cr_2S_3 increases approximately linearly in the pressure range from 2.8 GPa to 6.2 GPa, and this result indicates that Cr_2S_3 is in an elastic deformation state. The linear fitting equation of Cr_2S_3 in this work can be expressed as

$$t = -0.59267 + 0.43259 \times P. \tag{4}$$

In addition, at low pressure, the deviatoric stresses of Cr_2S_3 in this work are lower than those of NbB_2 derived by Xiong *et al.*[30] It can be inferred that the hardness of Cr_2S_3 is likely to be lower than that of NbB_2.

In summary, we have investigated the EOS of Cr_2S_3 at high pressures using synchrotron radiation and silicone oil as a pressure-transmitting medium in a DAC. We found that Cr_2S_3 undergoes a structural phase transition at 8.5 GPa. The bulk modulus of Cr_2S_3 obtained by fitting the structure at low pressure is 88 GPa. Correspondingly, the bulk modulus calculated by DFT is 67 GPa. In addition, we have investigated the electrical resistance of Cr_2S_3 at high pressures and different temperatures. With increasing pressure or temperature, the resistance first decreases rapidly and then remains almost constant, indicating that Cr_2S_3 undergoes a transition from semiconductor to metal. After decompression, Cr_2S_3 remains metallic. High-pressure Raman experiments show that the peak positions of peaks 1, 2 and 3 are red-shifted with increase in pressure, which may be due to the distortion of CrS_6 octahedra. The peak position of peak 4 increases approximately linearly at low pressure, but remains basically unchanged beyond 8 GPa. Therefore, we conclude that it is highly probable that Cr_2S_3 undergoes a structural phase transition at 8 GPa. Finally, the deviatoric stress of Cr_2S_3 at high pressures was investigated by the linewidth analysis method. The results show that at low pressure the strength of Cr_2S_3 increases approximately linearly. The deviatoric stress is 2.0 GPa at a pressure of 6 GPa.

Acknowledgements

We gratefully acknowledge the financial supported of the National Key Research and Development Program of China (Grant No. 2021YFB3702102), the National Natural Science Foundation of China (Grant No. 12374019), the Open Fund Project of the Research Institute of Intelligent Manufacturing Industry Technology of SiChuan Arts and Science University (Grant No. ZNZZ2503), and Key Laboratory of Intelligent Optoelectronic System Perception and Application in Sichuan Province, China (Grant No. ZNGD2219).

References

[1] Yuzuri M, Kanomata T and Kaneko T 1987 *J. Magn. Magn. Mater.* **70** 223
[2] Li C Y, Ke F, Hu Q Y, Yu Z H, Zhao J G, Chen Z Q and Yan H 2016 *J. Appl. Phys.* **119** 135901
[3] Yuzuri M and Nakamura Y 1964 *J. Phys. Soc. Jpn.* **19** 1350
[4] Mao H K, Xu J and Bell P M 1986 *J. Geophys. Res.* **91** 4673
[5] Hammersley A P, Svensson S O, Hanfland M, Fitch A N and Häusermann D 1996 *High Pressure Res.* **14** 235
[6] Liu J X, Yan J J, Shi Q W, Dong H L, Zhang J B, Wang Z W, Huang W X, Chen B and Zhang H Z 2019 *J. Phys. Chem. C* **123** 4094
[7] Kresse G and Furthmüller J 1996 *J. Comp. Mater. Sci.* **6** 15
[8] Perdew J P, Burke K and Ernzerhof M 1996 *Phys. Rev. Lett.* **77** 3865
[9] Blochl P E 1994 *Phys. Rev. B* **50** 17953
[10] Grimme S 2006 *J. Comput. Chem.* **27** 1787
[11] Xiong L, Liu J, Bai L G, Li Y C, Lin C L, He D W, Peng F and Lin J F 2013 *J. Appl. Phys.* **113** 033507
[12] Birch F 1978 *J. Geophys. Res.* **83** 12573
[13] Xiong L, Li Q, Yang C F, Xie Q S and Zhang J R 2020 *Chin. Phys. B* **29** 086401
[14] Duffy T S, Shen G Y, Heinz D L, Shu J F, Ma Y Z, Mao H K, Hemley R J and Singh A K 1999 *Phys. Rev. B* **60** 15063
[15] Golosova N O, Kozlenko D P, Kichanov S E, Lukin E V, Liermann H P, Glazyrin K V and Savenko B N 2017 *J. Alloys Compd.* **722** 593
[16] Mougin J, Bihan T L and Lucazeau G 2001 *J. Phys. Chem. Solids* **62** 553
[17] Pereiraet A L, Errandonea D, Beltran A, Gracia L, Gomis O, Sans J A, Garcia-Domene B, Miquel-Veyrat A, Manjon F J, Munoz A and Popescu C 2013 *J. Phys.: Condens. Matter* **25** 475402
[18] Efthimiopoulos I, Kemichick J, Zhou X, Khare S V, Ikuta D and Wang Y J 2014 *J. Phys. Chem. A* **118** 1713
[19] Li C Y, Zhao J G, Hu Q Y, Liu Z G, Yu Z H and Yan H 2016 *J. Alloys Compd.* **688** 329
[20] Pereira A L, Gracia L, Santamaria-Perez D, Vilaplana R, Manjon F J, Errandonea D, Nalin M and Beltran A 2012 *Phys. Rev. B* **85** 174108
[21] Lbanez J, Tresserras J A S, Popescu C, Lopez-Vidrier J, Betanzos J J E, Cuenca-Gotor V P, Gomis O, Manjon F J, Hernandez P R and Munoz A 2016 *J. Phys. Chem. C* **120** 10547
[22] Lundegaard L F, Miletich R, Balic T and Makovicky E 2003 *Phys. Chem. Minerals* **30** 463
[23] Palmer S B and Lee E 1971 *Philos. Mag.* **24** 311
[24] Lichnowski A J and Saunders G A 1976 *J. Phys. C* **9** 927
[25] Liu L, Song H X, Geng H Y, Bi Y, Xu J A, Li X D, Li Y C and Liu J 2013 *Phys. Status Solidi B* **250** 1398
[26] Jong M D, Chen W, Angsten T, Jain A, Notestine R, Gamst A, Sluiter M, Ande C K, Zwaag S, Plata J J, Toher C, Curtarolo S, Ceder G, Persson K A and Asta M 2015 *Sci. Data* **2** 15009
[27] Li, P, Xu C Y and Luo W D 2022 *Phys. Rev. Mater.* **6** 054006
[28] Yang Y, Bai L G, Zhu K, Liu Y L, Jiang S, Liu J, Chen J and Xing X R 2009 *J. Phys.: Condens. Matter* **21** 385901
[29] Konopkova Z, Rothkirc A, Singh A K, Speziale S and Liermann H P 2015 *Phys. Rev. B* **91** 144101
[30] Xiong L, Jiang M Q, Miao F and Jiang S 2024 *Solid State Commun.* **394** 115706